JOURNAL OF AIRCRAFT
Vol. 46, No. 4, July–August 2009

Optimum Design of a Compound Helicopter

Hyeonsoo Yeo* and Wayne Johnson†
NASA Ames Research Center, Moffett Field, California 94035

DOI: 10.2514/1.40101

A design and aeromechanics investigation was conducted for a 100,000 lb compound helicopter with a single main rotor that will cruise at a condition of 250 kt at 4000 ft/95°F. Performance, stability, and control analyses were conducted with the comprehensive rotorcraft analysis CAMRAD II. Wind-tunnel test measurements of the performance of the H-34 and UH-1D rotors at high advance ratios were compared with calculations to assess the accuracy of the analysis for the design of a high-speed helicopter. In general, good correlation was obtained with the test data. An assessment of various design parameters (disk loading, blade loading, wing loading) on the performance of the compound helicopter was made. Lower wing loading (larger wing area) and higher design blade loading (smaller blade chord) increased the aircraft lift-to-drag ratio. However, disk loading has a small influence on the aircraft lift-to-drag ratio. A rotor parametric study showed that most of the benefit of slowing the rotor occurred at the initial 20–30% reduction of the advancing blade tip Mach number. No stability issues were observed with the current design, and the control derivatives did not change much with speed, but did exhibit significant coupling.

Nomenclature

A	=	rotor disk area
C_L	=	rotor lift coefficient
C_P	=	rotor power coefficient
C_{P_i}	=	rotor induced power coefficient
C_{P_o}	=	rotor profile power coefficient
C_T	=	rotor thrust coefficient
C_W	=	weight coefficient
C_X	=	rotor propulsive force coefficient
D/q	=	airframe drag divided by dynamic pressure
EI_{flap}	=	flap bending stiffness
EI_{lag}	=	lag bending stiffness
GJ	=	torsion stiffness
I_P	=	section polar moment of inertia
I_θ	=	section moment of inertia
L/D_e	=	aircraft effective lift-to-drag ratio, WV/P
M	=	Mach number
M_{at}	=	advancing tip Mach number
P	=	aircraft power
R	=	rotor radius
S	=	wing area
V	=	flight speed
W	=	gross weight
W/A	=	disk loading
W/S	=	wing loading
x_{EA}	=	chordwise elastic axis relative reference axis (positive toward trailing edge)
x_I	=	chordwise center of gravity offset relative elastic axis (positive toward trailing edge)
α_s	=	shaft tilt angle (positive for rearward tilt)
α_w	=	wing incidence angle
μ	=	advance ratio
ν_β	=	blade fundamental flap frequency
ν_ζ	=	blade fundamental lag frequency
σ	=	solidity (thrust weighted)

Received 28 July 2008; revision received 19 December 2008; accepted for publication 24 January 2009.

*Research Scientist, Aeroflightdynamics Directorate, U.S. Army Research, Development, and Engineering Command, Mail Stop 215-1; hyeonsoo.yeo@us.army.mil. Member AIAA.

†Research Scientist, Flight Vehicle Research and Technology Division, Mail Stop 243-12. Fellow AIAA.

Introduction

RECENTLY, the NASA Heavy Lift Rotorcraft Systems Investigation was conducted to identify candidate configurations for a large civil vertical takeoff and landing transport that is technically promising and economically competitive [1]. The vehicle was required to carry 120 passengers over a range of 1200 n mile and cruise at 350 kt at an altitude of 30,000 ft. A large civil tandem compound (LCTC) helicopter was designed as one of the candidate configurations to meet this NASA 15-year notional capability [2]. This study also revealed the need to further investigate the aeromechanics issues of a compound helicopter.

A compound helicopter is one solution to achieving high-speed capability while retaining the hover advantages of a helicopter. In general, the lifting and propulsive force capabilities of a helicopter rotor decrease with forward speed as a result of asymmetric flow conditions encountered by the rotor. A compound helicopter circumvents the rotor lift limit by adding wings to the fuselage (lift compounding) and the rotor propulsive limit by adding additional propulsive devices (propulsive thrust compounding). The compound helicopter investigated in this paper is defined as a helicopter with both a wing and an auxiliary propulsion (fully compounding). To maintain low rotor drag at high speed, it is necessary to slow the rotor, in part to minimize the compressible drag rise on the advancing blade.

In this paper, a design and aeromechanics investigation was conducted for a 100,000 lb compound helicopter with a single main rotor that will cruise at a condition of 250 kt at 4000 ft/95°F (Fig. 1). In contrast, the LCTC [2] was designed for a much higher speed and altitude. This paper presents the rotor performance correlation at high speeds and the results of the compound helicopter design investigation. A parametric study was conducted to understand the effects of design parameters on the performance of the aircraft. Stability and control issues were also investigated.

CAMRAD II Modeling

Performance, loads, and stability analyses were conducted with the comprehensive rotorcraft analysis CAMRAD II [3]. CAMRAD II is an aeromechanics analysis of rotorcraft that incorporates a combination of advanced technologies, including multibody dynamics, nonlinear finite elements, and rotorcraft aerodynamics. The trim task finds the equilibrium solution for a steady-state operating condition and produces the solution for performance, loads, and vibration. The flutter task linearizes the equations about the trim solution and produces the stability results. The aerodynamic model includes a wake analysis to calculate the rotor nonuniform induced velocities using rigid, prescribed, or free wake geometry.

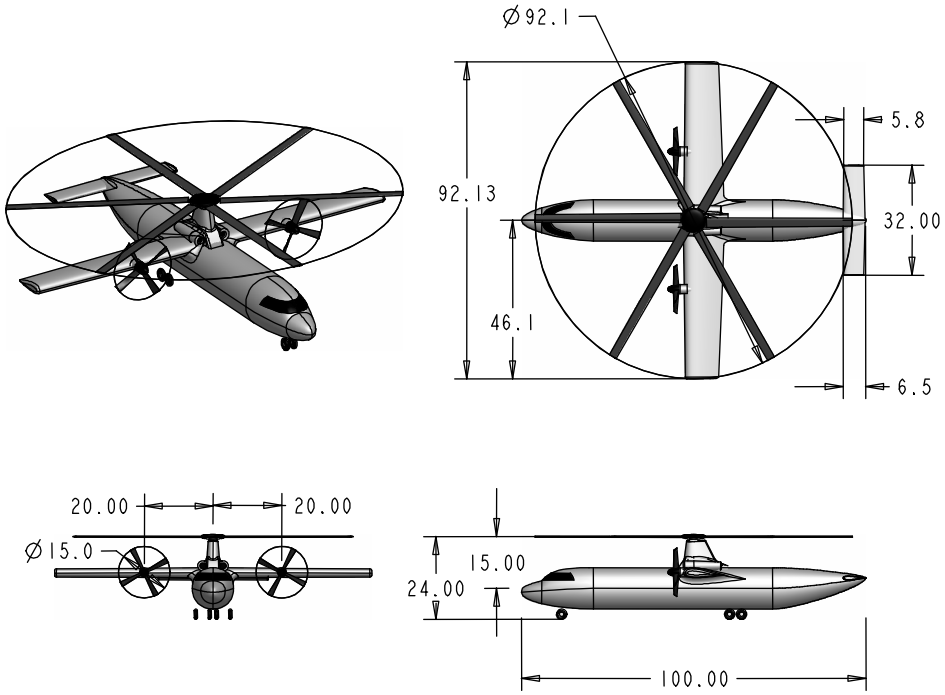

Fig. 1 Three-view drawing of the compound helicopter; dimensions are in feet (courtesy Gerardo Nunez of the U.S. Army Aeroflightdynamics Directorate).

CAMRAD II has undergone extensive correlation of performance and loads measurements on helicopters [4–6].

A complete aeroelastic model was developed for the analysis of the compound helicopter. The comprehensive analysis modeled the auxiliary propulsion as forces applied to the airframe. Rotor/wing interference was accounted for using a vortex wake model for both the rotor and the wing. For all the calculations made in this study, an elastic blade model was used, scaled from the LCTC blade design. Rotor performance was calculated using nonuniform inflow with prescribed wake geometry in high-speed cruise and free wake geometry in hover.

In cruise, the aircraft was trimmed using lateral stick to the ailerons, longitudinal stick to the elevator, and pedal to differential propeller thrust, plus propeller thrust and aircraft pitch and roll angles. The rotor collective pitch angle was set to values optimized for cruise performance (optimized rotor thrust). In addition to the three force and three moment equilibrium of the aircraft, rotor hub roll and pitch moments were trimmed to zero (for load control) using rotor cyclic pitch; thus, there were eight trim variables for cruise.

Rotor Performance Correlation at High Speed

The ability to accurately predict the performance of a helicopter is essential for the design of future rotorcraft. It is necessary to assess the accuracy and reliability of these prediction methods, with the ultimate goal of providing the technology for the timely and cost-effective design and development of new rotors.

Wind-tunnel test data of the full-scale H-34 rotor [7] and UH-1D rotor [8] obtained in the late 1960s provide a set of test conditions at high advance ratios. A full-scale H-34 articulated rotor with zero twist blades was tested in the NASA Ames 40×80 ft wind tunnel. Tunnel speed and rotor rotational speed were adjusted to obtain the desired advance ratio and advancing tip Mach number. At each combination of shaft tilt angle and collective pitch, the cyclic pitch was adjusted to minimize first harmonic blade flapping. A full-scale UH-1D teetering rotor with -1.42 deg twist blades, reduced in diameter to 34 ft, was tested in the NASA Ames 40×80 ft wind tunnel. The test procedure was same as for the H-34 rotor test. Both rotors used a NACA 0012 airfoil.

Rotor performance calculations with CAMRAD II are compared with the wind-tunnel test data in Figs. 2 and 3. Detailed rotor blade structural and inertial properties used in the analysis are in Tables 1 and 2. The current analysis models have been updated from the previous study [9] to include the H-34 inboard blade shank and the UH-1D blade root doubler. The H-34 inboard blade shank was modeled as constant drag ($c_d = 0.114$) with a chord of 0.6 ft over $r/R = 0.08$–0.16. For the UH-1D rotor, the doubler drag increment was modeled as delta c_d of 0.015 over $r/R = 0.12$–0.38. It should be

Table 1 H-34 rotor blade properties

r/R	Mass, slug/ft	EI_{flap}, lb · ft^2	EI_{lag}, lb · ft^2	GJ, lb · ft^2	I_θ, slug · ft	I_p, slug · ft	x_{EA} x/R	x_I x/R
0.000	2.0500	5.40E + 5	6.50E + 6	8.30E + 5	0.1290	0.1290	0.0	0.0
0.033	2.0500	5.40E + 5	6.50E + 6	8.30E + 5	0.1290	0.1290	0.0	0.0
0.038	2.0500	1.04E + 6	1.74E + 6	8.30E + 5	0.1290	0.1290	0.0	0.0
0.049	2.0500	3.47E + 6	3.21E + 6	8.30E + 5	0.1290	0.1290	0.0	0.0
0.068	1.7700	3.47E + 6	3.21E + 6	8.30E + 5	0.0680	0.0680	0.0	0.0
0.082	0.6120	2.23E + 6	6.40E + 5	3.10E + 5	0.0480	0.0480	0.0	0.0
0.093	0.3990	1.10E + 6	2.36E + 6	3.10E + 5	0.0230	0.0230	0.0	0.0
0.109	0.1310	2.10E + 5	1.39E + 6	1.53E + 5	0.0060	0.0060	0.0	0.0
0.150	0.1310	1.19E + 5	1.19E + 6	1.46E + 5	0.0120	0.0120	0.0	0.0
0.199	0.1570	1.19E + 5	1.19E + 6	1.39E + 5	0.0160	0.0160	0.0	0.0
0.219	0.2050	1.02E + 5	1.11E + 6	1.25E + 5	0.0175	0.0175	0.0	0.0
0.861	0.2050	1.02E + 5	1.11E + 6	1.25E + 5	0.0175	0.0175	0.0	0.0
0.885	0.3540	1.02E + 5	1.11E + 6	1.25E + 5	0.0175	0.0175	0.0	0.0
1.000	0.0930	1.02E + 5	1.11E + 6	1.25E + 5	0.0175	0.0175	0.0	0.0

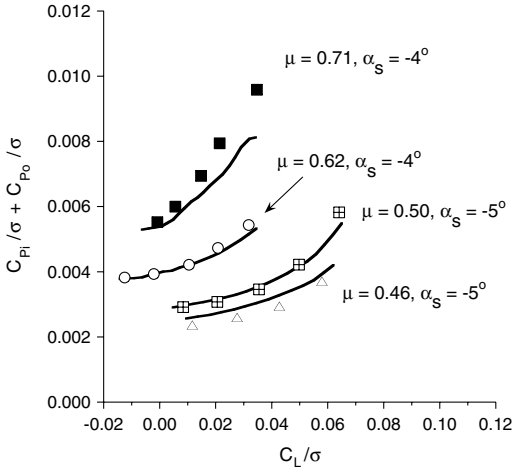

a) around α_s = -5 deg

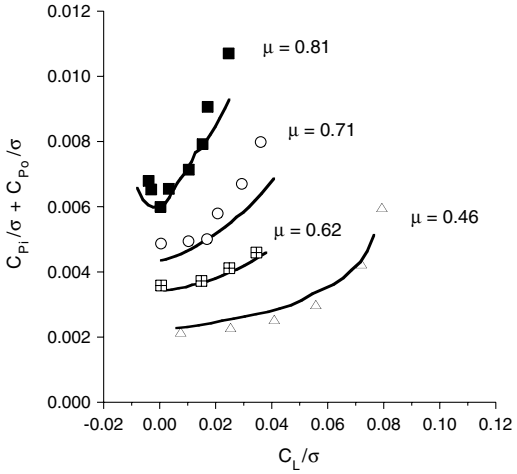

b) α_s = 0 deg

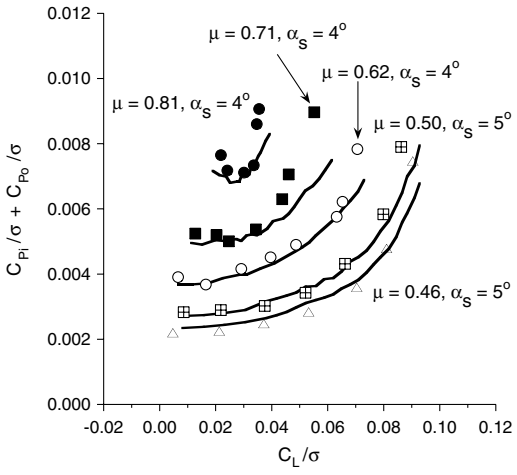

c) around α_s = 5 deg

Fig. 2 H-34 rotor performance correlation (symbols: wind-tunnel test, lines: analysis).

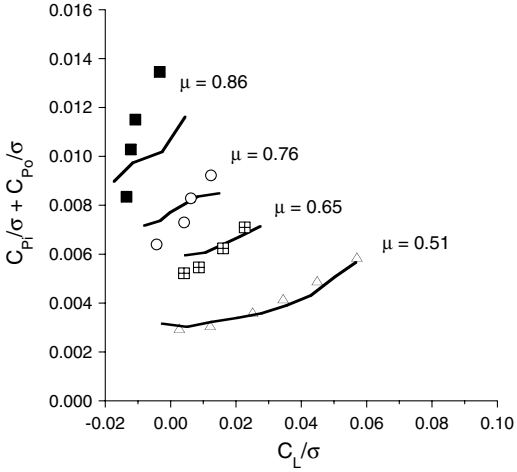

a) α_s = -4 deg

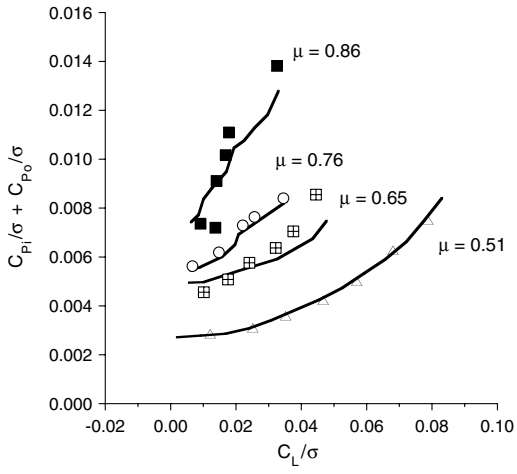

b) α_s = 0 deg

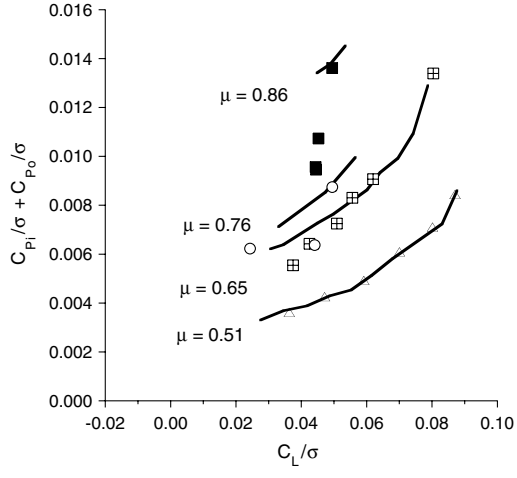

c) α_s = 4 deg

Fig. 3 UH-1D rotor performance correlation (symbols: wind-tunnel test, lines: analysis).

noted that the shank drag and doubler drag increments were estimated based on correlation as no independent data on drag of shank or doubler were available.

Figure 2 shows the rotor induced power plus profile power versus rotor lift for the H-34 rotor for three different shaft tilt angles. The wind-tunnel data for rotor induced power plus profile power were obtained from the total rotor power coefficient and rotor propulsive coefficient measurements, $C_{P_i} + C_{P_O} = C_P - C_X\mu$. Rotor performance was calculated using nonuniform inflow with free wake geometry and unsteady aerodynamics. Section lift, drag, and moment values for the NACA 0012 airfoil were obtained from an airfoil table, including data over a full 360 deg range of angle of attack. Reverse and yawed flows are important for the rotor performance correlation at high advance ratios, and the current analysis included both. Reverse flow occurs when the blade section velocity is negative or when the angle of attack is greater than ±90 deg. The

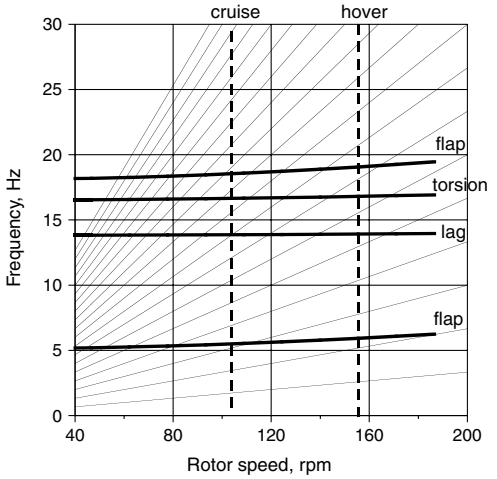

Fig. 4 Blade frequencies (with a collective angle of 10 deg).

sign conventions in reverse flow are consistent with the definition of the angle of attack in the airfoil tables. Yawed flow over the blade section was accounted for using effective dynamic pressure and the angle of attack of the yawed section and an estimate of the radial drag. However, a dynamic stall model was not used in the performance calculations as the previous analytical investigation [10] showed that dynamic stall models, in general, had only a small influence on the rotor power predictions.

The rotor induced power plus profile power increases as the advance ratio increases for the same rotor lift and as rotor lift increases for the same advance ratio. The analysis shows, in general, good correlation with the measurements. Underprediction of rotor power at high rotor lift was observed. It appears that the current analysis or airfoil table used has optimistic stall characteristics. Dynamic stall is not considered likely to be a factor at these operating conditions.

Figure 3 shows the rotor induced power plus profile power versus rotor lift for the UH-1D rotor for three different shaft tilt angles. The analysis shows reasonably good correlation at all the advance ratios investigated for $\alpha_s = 0$ deg. For the $\alpha_s = \pm 4$ deg cases, the analysis shows good correlation for $\mu = 0.51$. However, the analysis overpredicts at low rotor lift and underpredicts at high rotor lift.

Aircraft Design Study

An assessment of various compound helicopter designs was made to understand the effects of design parameters on the performance of the aircraft and to define a baseline model for an aeromechanics study. The compound helicopter configuration developed in this study is shown in Fig. 1. The aircraft has a six-bladed rotor, a high wing, a horizontal tail, and two auxiliary propellers located on the wing for cruise propulsion and antitorque in hover. State-of-the-art rotor airfoils (VR-12 and SSCA09) were used for the main rotor blades.

A hingeless rotor hub was used. Blade inertial and structural properties were scaled from the blade developed from the LCTC [2]. Figure 4 shows the calculated blade frequencies at a collective pitch angle of 10 deg. At helicopter-mode tip speed, the first flap frequency was about 2.3/rev, the first lag frequency was about 5.4/rev, and the first torsion frequency was about 6.5/rev.

The current compound helicopter has a very stiff rotor, and its fuselage and wing were assumed rigid in the analysis. Thus, structural dynamics are not a significant factor in the aerodynamic performance shown in this paper. A stiff hingeless rotor is considered a good design choice, if innovative solutions are found to keep rotor weight reasonable. In any case, it allows this paper to focus on aerodynamic performance. Rotor and wing planform, twist optimization, and the principal characteristics of airfoils are the key

Table 2 UH-1D rotor blade properties

r/R	Mass, slug/ft	EI_{flap}, lb · ft^2	EI_{lag}, lb · ft^2	GJ, lb · ft^2	I_θ, slug · ft	I_p, slug · ft	x_{EA} x/R	x_I x/R
0.000	4.9689	5.24E + 7	2.32E + 8	1.17E + 8	0.9427	0.5611	−0.0056	0.0000
0.017	4.9689	5.24E + 7	2.32E + 8	1.17E + 8	0.9427	0.5611	−0.0056	0.0000
0.030	2.4559	2.95E + 7	7.27E + 7	1.83E + 7	0.3826	0.1674	−0.0056	0.0067
0.043	0.7751	2.43E + 6	5.63E + 7	4.81E + 5	0.2088	0.1908	−0.0059	0.0120
0.050	0.5139	1.06E + 6	3.43E + 7	3.83E + 5	0.1325	0.1242	−0.0060	0.0109
0.058	0.4954	1.01E + 6	3.13E + 7	3.76E + 5	0.1582	0.0790	−0.0061	0.0104
0.084	0.4660	9.12E + 5	2.87E + 7	3.64E + 5	0.1127	0.1055	−0.0064	0.0102
0.108	0.4252	7.69E + 5	2.61E + 7	3.53E + 5	0.1302	0.0686	−0.0067	0.0103
0.127	0.3863	6.33E + 5	2.46E + 7	3.31E + 5	0.0963	0.0911	−0.0070	0.0106
0.144	0.3567	5.44E + 5	2.35E + 7	3.12E + 5	0.0915	0.0871	−0.0073	0.0107
0.157	0.3345	4.77E + 5	2.30E + 7	2.97E + 5	0.0892	0.0854	−0.0075	0.0111
0.177	0.3119	4.22E + 5	2.12E + 7	2.89E + 5	0.0827	0.0792	−0.0077	0.0109
0.194	0.2896	3.65E + 5	2.04E + 7	2.82E + 5	0.0796	0.0766	−0.0080	0.0114
0.211	0.2721	3.24E + 5	1.98E + 7	2.52E + 5	0.0770	0.0743	−0.0083	0.0119
0.226	0.2567	2.92E + 5	1.91E + 7	2.46E + 5	0.0743	0.0719	−0.0085	0.0124
0.261	0.2417	2.66E + 5	1.81E + 7	2.36E + 5	0.0707	0.0685	−0.0085	0.0127
0.299	0.2387	2.66E + 5	1.70E + 7	2.15E + 5	0.0674	0.0653	−0.0084	0.0120
0.336	0.2357	2.65E + 5	1.59E + 7	2.08E + 5	0.0641	0.0619	−0.0083	0.0113
0.373	0.2328	2.65E + 5	1.48E + 7	2.02E + 5	0.0608	0.0586	−0.0082	0.0106
0.410	0.1970	2.09E + 5	1.34E + 7	1.87E + 5	0.0549	0.0532	−0.0081	0.0117
0.448	0.1946	2.08E + 5	1.25E + 7	1.80E + 5	0.0520	0.0503	−0.0080	0.0109
0.485	0.1922	2.08E + 5	1.15E + 7	1.74E + 5	0.0490	0.0473	−0.0079	0.0102
0.522	0.1901	2.08E + 5	1.06E + 7	1.71E + 5	0.0462	0.0445	−0.0078	0.0096
0.601	0.1872	2.08E + 5	9.42E + 6	1.71E + 5	0.0421	0.0404	−0.0077	0.0086
0.672	0.2239	2.09E + 5	8.40E + 6	1.71E + 5	0.0429	0.0412	−0.0074	0.0042
0.709	0.2219	2.09E + 5	7.58E + 6	1.71E + 5	0.0394	0.0376	−0.0073	0.0036
0.746	0.2213	2.09E + 5	7.30E + 6	1.71E + 5	0.0382	0.0365	−0.0072	0.0033
0.821	0.2214	2.09E + 5	7.30E + 6	1.71E + 5	0.0386	0.0369	−0.0070	0.0032
0.896	0.2217	2.09E + 5	7.30E + 6	1.71E + 5	0.0390	0.0373	−0.0068	0.0030
0.938	0.2327	2.23E + 5	7.70E + 6	1.76E + 5	0.0401	0.0383	−0.0067	0.0023
0.950	0.3983	2.23E + 5	7.70E + 6	1.76E + 5	0.0401	0.0383	−0.0066	0.0023
0.980	0.6300	4.32E + 5	8.36E + 6	5.23E + 5	0.0415	0.0383	−0.0065	0.0029
1.000	0.2327	2.23E + 5	7.70E + 6	1.76E + 5	0.0401	0.0383	−0.0065	0.0021

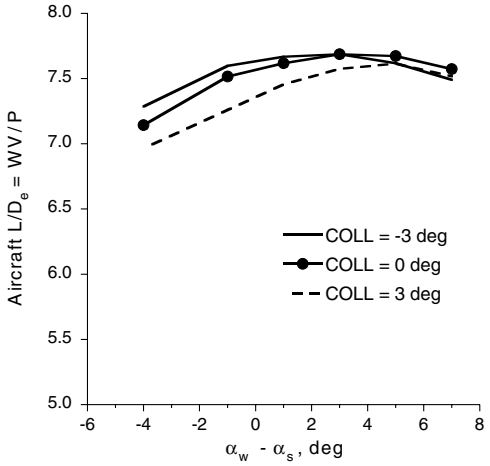

a) Wing loading (W/S) = 100

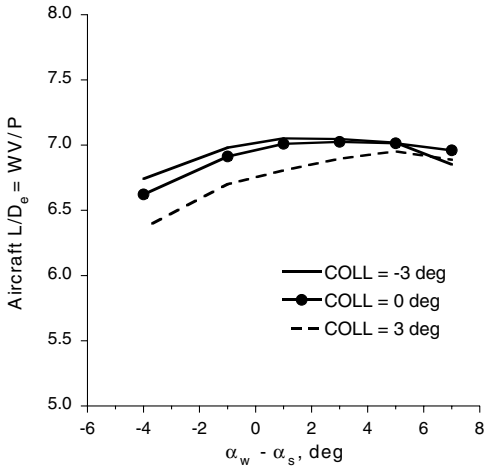

b) Wing loading (W/S) = 120

Fig. 5 Effect of wing loading on the aircraft lift-to-drag ratio ($W/A = 15$, $C_W/\sigma = 0.14$).

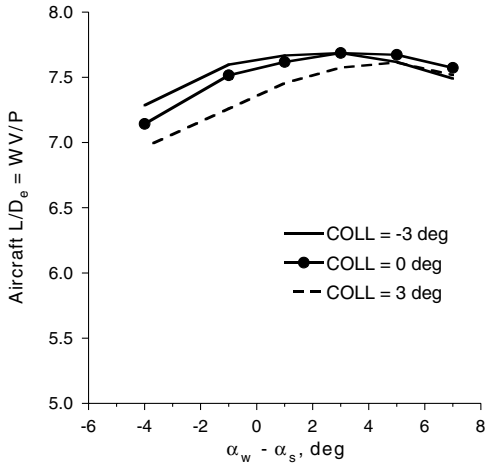

a) Blade loading (C_W/σ) = 0.14

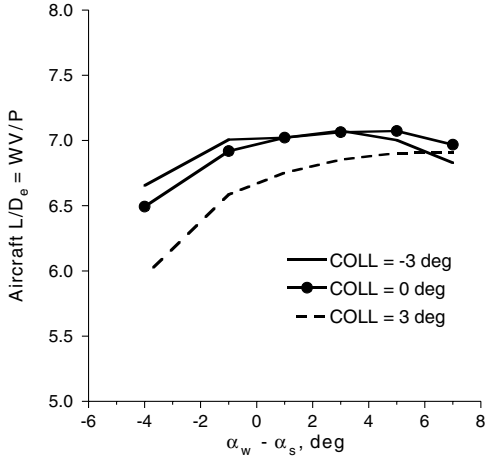

b) Blade loading (C_W/σ) = 0.09

Fig. 6 Effect of blade loading on the aircraft lift-to-drag ratio ($W/A = 15$, $W/S = 100$).

information required to produce or replicate the aerodynamic performance results shown in this paper.

Table 3 shows the design parameters investigated. The baseline aircraft design parameters (Fig. 1) are disk loading of $W/A =$ 15 lb/ft^2, blade loading of $C_T/\sigma = 0.14$, and wing loading of $W/S = 100$ lb/ft^2. This design was the optimum design for the LCTC, and is shown here to give good performance for the present aircraft. The $C_T/\sigma = 0.14$ and $W/S = 100$ are appropriate for an aircraft that unloads the rotor at a relatively low speed. The aircraft parasite drag is $D/q = 40.5$ ft^2. This drag value, which was obtained from historic trends [2], is higher than current turboprop aircraft, but lower than is customary in the helicopter industry. The baseline design has a wingspan equal to the rotor diameter (Fig. 1). The hover tip speed is 750 ft/s and the cruise tip speed is 502 ft/s, which gives $M_{at} = 0.8$ at 250 kt. The advance ratio is then $\mu = 0.84$ at 250 kt.

Design variations of wing loading ($W/S = 100$ vs 120), blade loading ($C_T/\sigma = 0.14$ vs 0.09), and disk loading ($W/A = 15$ vs 12) were examined. The larger disk area will give lower hover power. The larger blade area or smaller wing area correspond to loading the rotor rather than the wing. Note that $C_T/\sigma = 0.09$ would be appropriate for a helicopter using advanced technology airfoils or active control; hence, the rotor could carry the aircraft weight to conventional helicopter speeds.

Figures 5–7 show the performance results in terms of aircraft lift-to-drag ratio $L/D_e = WV/P$, calculated without accessory or other losses and using a propeller efficiency of 0.86, all for the design cruise condition of 250 kt. The power in the aircraft lift-to-drag ratio equation consists of rotor power and auxiliary power. The auxiliary power is defined as auxiliary force times flight speed divided by

Table 3 Compound helicopter design parameters

Parameters independent of design conditions				
Operating condition, ft/°F	4000/95			
Cruise speed, kt	250			
Mission GW (lb)	100,000			
Tip speed, hover, ft/s	750			
Tip speed, cruise, ft/s	502			
Drag D/q, ft^2	40.5			
Drag, $(D/q)/(W/1000)^{2/3}$	1.9			
Number of blades	6			
Taper ratio (blade, wing)	0.8			
Parameters dependent on design conditions				
Disk loading W/A, lb/ft^2	15	15	12	12
Rotor diameter, ft	92.13	92.13	103.01	103.01
Blade loading (C_W/σ)	0.14	0.09	0.14	0.09
Solidity	0.0992	0.1543	0.0794	0.1235
Chord (75%R), ft	2.39	3.72	2.14	3.33
Aspect ratio	19.25	12.38	24.06	15.47
Wing loading W/S, lb/ft^2	100	120		
Area, ft^2	1000	833		
Span, ft	92.13	76. 78		
Chord (75%R), ft	10.25	10.25		
Aspect ratio	8.49	7.07		

propeller efficiency. Thus, $P = P_{\text{rotor}} + P_{\text{aux}} = P_{\text{rotor}} + F_{\text{aux}} V/\eta$, where F_{aux} is the auxiliary force and η is the propeller efficiency. For each combination of disk loading, design blade loading, and wing loading, three collective angles (−3, 0, and 3 deg) and six values for the difference between wing incidence and shaft tilt angle ($\alpha_w - \alpha_s = -4, -1, 1, 3, 5$, and 7 deg) were used. Although wing incidence and shaft tilt angle can be set independently, their relative position determines aircraft pitch attitude in a trimmed condition to have a unique lift sharing between rotor and wing for a given collective angle. For example, the aircraft with $\alpha_w = 3$ deg and $\alpha_s = 0$ deg and the aircraft with $\alpha_w = 0$ deg and $\alpha_s = -3$ deg (which means a 3 deg forward tilt) will be trimmed in such a way that rotor and wing angles of attack are same for both cases. The rotor rpm was 104.0 to obtain $M_{\text{at}} = 0.8$.

Figure 5 shows the effect of wing loading ($W/S = 100$ vs 120) on the aircraft lift-to-drag ratio for $W/A = 15$ and $C_T/\sigma = 0.14$. To obtain higher wing loading, the wing area was reduced by decreasing the wing span for a given chord. The aircraft lift-to-drag ratio increases as the $\alpha_w - \alpha_s$ increases (the wing incidence increases or the rotor shaft tilts forward) up to 3 deg for the collective angle of 0 and −3 deg and up to 5 deg for the collective angle of 3 deg and then decreases. The best performance was obtained for the collective angle of 0 or −3 deg and $\alpha_w - \alpha_s = 3$ deg. Lower wing loading (a higher wing area) increased the aircraft lift-to-drag ratio. The smaller wing area corresponds to loading the rotor rather than the wing. The wing is a more efficient lifting device than the rotor for the current 250 kt compound helicopter; thus, the larger wing area improves the aircraft performance.

Figure 6 shows the effect of blade loading ($C_T/\sigma = 0.14$ vs 0.09) on the aircraft lift-to-drag ratio for $W/A = 15$ and $W/S = 100$. To obtain lower blade loading, the blade area was increased by increasing the blade chord for a given blade radius. Thus, solidity was increased but aspect ratio was decreased. The larger blade area corresponds to loading the rotor rather than the wing. Higher design blade loading (smaller blade chord) increased the aircraft lift-to-drag ratio because the smaller blade chord reduced the rotor profile power.

Figure 7 shows the effect of disk loading ($W/A = 15$ vs 12) on the aircraft lift-to-drag ratio for $W/S = 100$ and $C_T/\sigma = 0.14$. To obtain lower disk loading, the rotor diameter was increased, but, to maintain the same blade loading for the increased rotor diameter, blade chord was decreased. Thus, the blade areas are identical for the two cases. Disk loading has a small influence on the aircraft performance, although it will have an impact on the rotor weight. Because the smaller blade chord increased the aircraft lift-to-drag ratio, as shown in Fig. 6, the larger rotor diameter must have decreased the aircraft lift-to-drag ratio as much as the increased aircraft lift-to-drag ratio by the smaller chord. The same blade area appears to result in the same aircraft performance.

The optimum required rotor shaft power and optimum lift sharing between the rotor and wing were investigated for the baseline aircraft ($W/A = 15$, $C_T/\sigma = 0.14$, and $W/S = 100$) at a cruise speed of 250 kt, and the results are shown in Figs. 8 and 9. Figure 8 shows the rotor shaft power for the baseline aircraft. The rotor power increases as $\alpha_w - \alpha_s$ increases. The required rotor power at the optimum aircraft lift-to-drag ratio occurred with a small, positive shaft power to the rotors: between 600 and 800 hp. With the rotor in autorotation

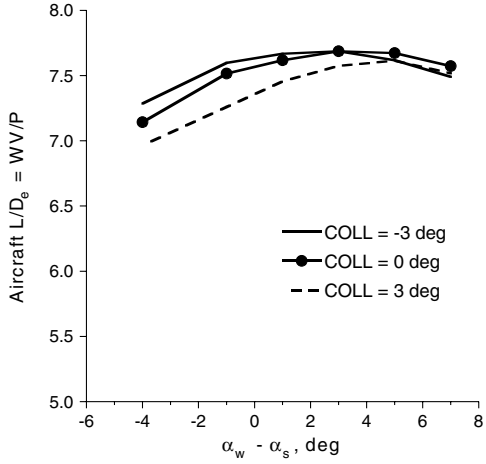

a) Disk loading (W/A) = 15

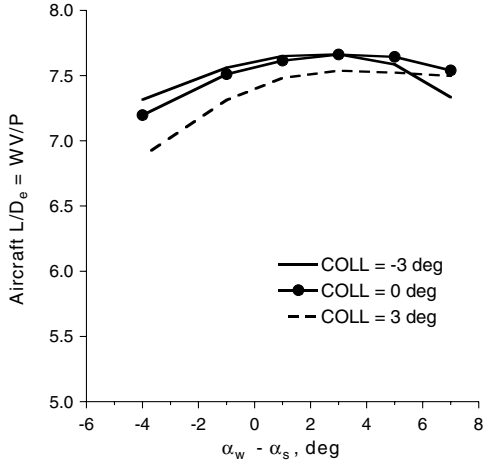

b) Disk loading (W/A) = 12

Fig. 7 Effect of disk loading on the aircraft lift-to-drag ratio ($C_W/\sigma = 0.14$, $W/S = 100$).

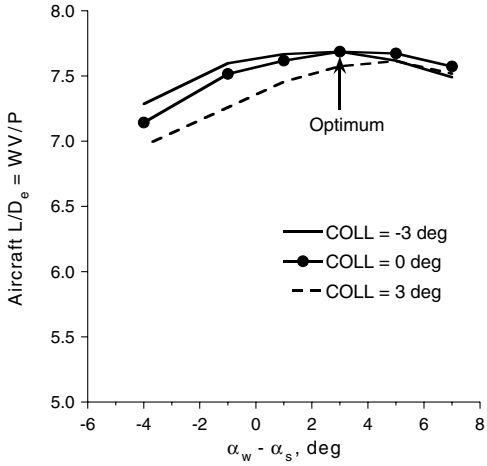

a) Aircraft lift-to-drag ratio

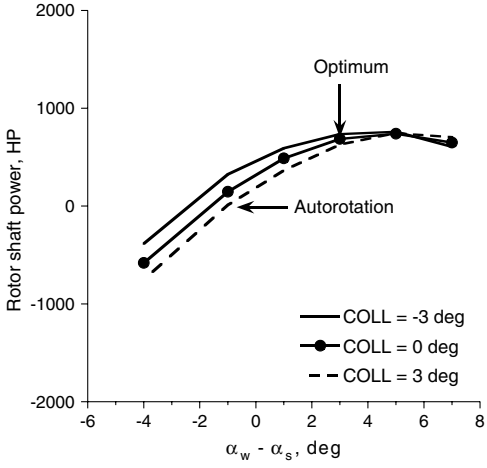

b) Rotor shaft power

Fig. 8 Rotor shaft power ($W/A = 15$, $C_W/\sigma = 0.14$, and $W/S = 100$).

(zero rotor shaft power), the rotor thrust was large; hence, the total rotor drag was larger and the aircraft L/D was somewhat smaller.

Figure 9 shows the rotor and wing lift for the baseline aircraft. As the $\alpha_w - \alpha_s$ increases, the rotor lift decreases and the wing lift increases. The higher collective angle increases the rotor lift and decreases the wing lift. The optimum lift sharing between the rotor and wing for the baseline aircraft is as follows: the rotor carries 8–9% of the aircraft gross weight and the wing carries 91–92% of the aircraft gross weight. The optimum lift sharing between the rotor and wing varied depending on disk loading, design blade loading, and wing loading. The rotor needs to carry more lift as the wing loading increases and the design blade loading decreases, as shown in Fig. 10.

Performance results for the baseline aircraft are shown in Figs. 11 and 12. The hover figure of merit of an isolated rotor is calculated with a 750 ft/s tip speed, and the result is shown in Fig. 11. The calculation was conducted using nonuniform inflow with free wake geometry. The figure of merit decreases as the thrust increases. This decrease was caused by an increase in profile power, as rotor stall was encountered at higher thrust. The figure of merit is around 0.78 at the design thrust ($C_T/\sigma = 0.1484$ with assumed 6% hover download). Figure 12 shows the aircraft lift-to-drag ratio with different airspeeds. The calculation was conducted using nonuniform inflow with a prescribed wake geometry. The airspeed was varied from 200 to 350 kt, with the rotor tip speed linearly decreased from hover. The aircraft lift-to-drag ratio decreases as airspeed goes up. At the design cruise speed (250 kt), the aircraft lift-to-drag ratio is 7.69.

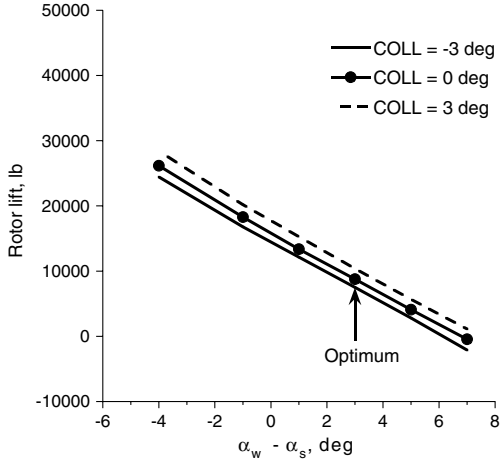

a) Rotor lift

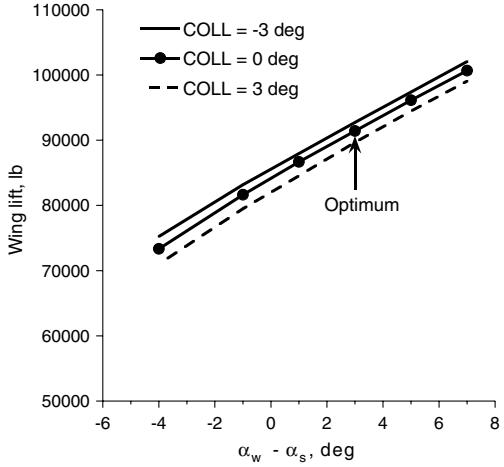

b) Wing lift

Fig. 9 Optimum lift sharing ($W/A = 15$, $C_W/\sigma = 0.14$, and $W/S = 100$).

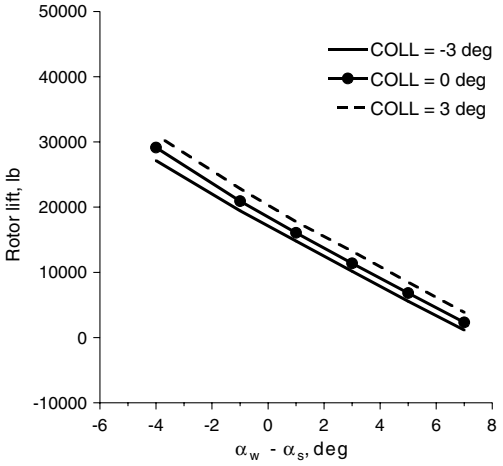

a) W/A = 15, C_W/σ = 0.14, W/S = 120

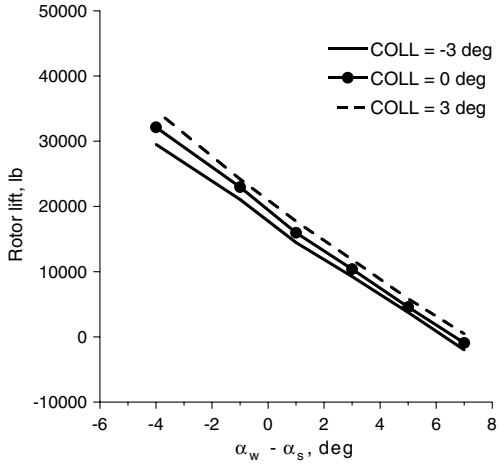

b) W/A = 15, C_W/σ = 0.09, W/S = 100

Fig. 10 Rotor lift variation.

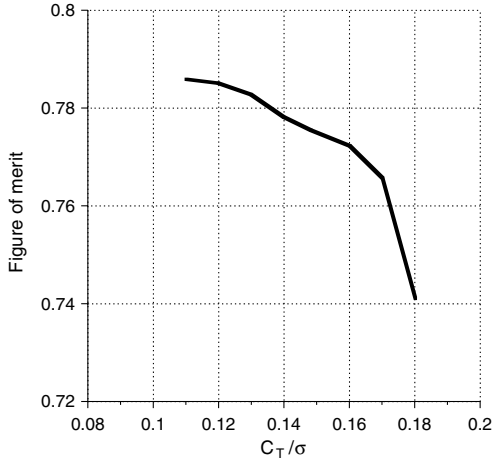

Fig. 11 Hover figure of merit.

Rotor Parametric Study

This section describes a parametric study of key rotor design parameters conducted with the comprehensive analysis. The baseline design was disk loading of 15, design blade loading of 0.14, wing loading of 100, collective angle of 0 deg, and $\alpha_w - \alpha_s$ of 3 deg.

The blade twist was varied to obtain balanced hover and cruise performance. The hover condition was a 750 ft/s tip speed, $C_T/\sigma = 0.1484$ (assumed 6% download). The cruise condition was 250 kt,

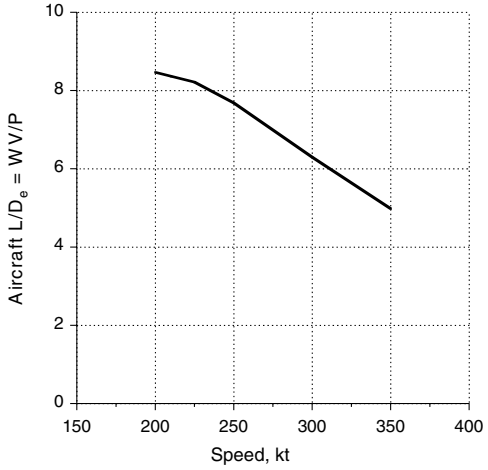

Fig. 12 Aircraft lift-to-drag ratio.

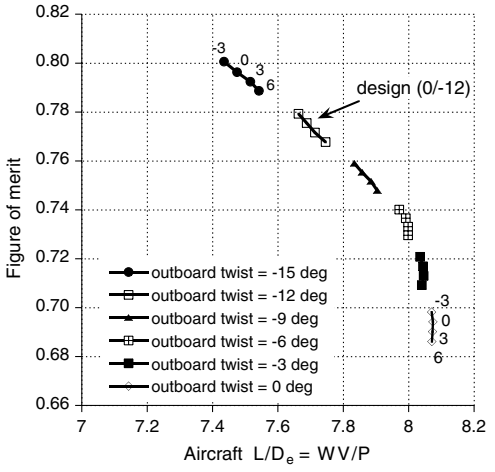

Fig. 13 Effect of blade twist on performance (inboard twist = −3, 0, 3, and 6 deg).

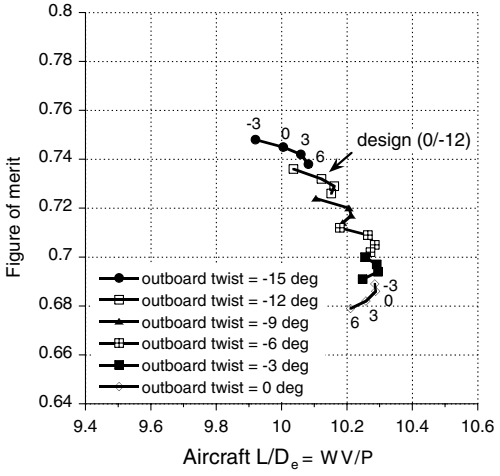

Fig. 14 Effect of blade twist on performance of LCTC (inboard twist = −3, 0, 3, and 6 deg) [Ref. [2]].

502 ft/s tip speed. The twist distribution had two linear segments, inboard (0.0–0.5R) and outboard (0.5–1.0R). Figure 13 presents the results for twist variation. For each value of outboard twist (−15, −12, −9, −6, −3, and 0 deg), the inboard twist values are −3, 0, 3, and 6 deg. A large negative twist improves hover performance, but the zero twist gives the best cruise performance. The design twist of 0 deg inboard and −12 deg outboard was selected based on the hover-cruise compromise. The result shows that the aircraft lift-to-drag ratio varies by 0.64 and the hover figure of merit varies by 0.115 within the twist range investigated. These variations are larger for the current design than those for the LCTC, as shown in Fig. 14 (aircraft lift-to-drag ratio varies by 0.37 and hover figure of merit varies by 0.069) and developed in [2]. Thus, the blade twist is a more important parameter for the current design than for the LCTC. However, the aircraft lift-to-drag ratio is less sensitive to the inboard twist change for the fixed outboard twist. Thus, the benefit of bilinear twist diminished for the current design compared with the LCTC.

Figure 15 shows the effects of the rotor advancing tip Mach number on the high-speed cruise (250 kt) performance. The rotor advancing tip Mach number was varied from 0.5 to 0.9 by changing the rotor rotational speed. It should be noted that the rotor advancing tip Mach number in cruise is about 1.02 with the hover tip speed. To maintain low rotor drag at high speeds, it is necessary to slow the rotor. The aircraft lift-to-drag ratio increases as the advancing tip Mach number decreases, reaching the maximum at $M_{at} = 0.55$, which corresponds to $\mu = 1.98$. Most of the benefit of slowing the rotor occurs at the initial 20–30% reduction of advancing blade-tip Mach number. The design point was found at $M_{at} = 0.80$, which corresponds to $\mu = 0.84$. This value corresponds to about a 20% reduction of advancing blade-tip Mach number and a 33% reduction of rotor tip speed from the hover condition.

The blade taper ratio was varied, as shown in Fig. 16. The taper model considered was a linear taper with a constant thrust-weighted solidity (chord at 75%R). The aircraft lift-to-drag ratio decreased as

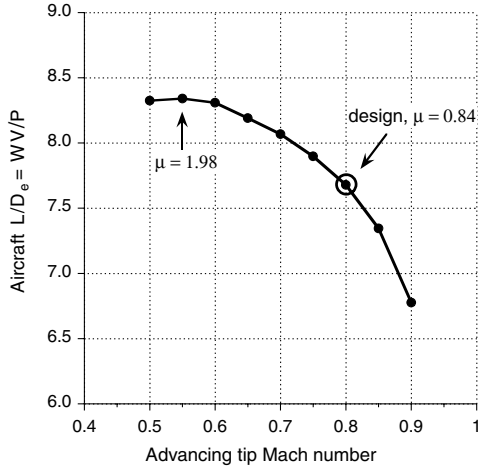

Fig. 15 Effect of tip speed on performance.

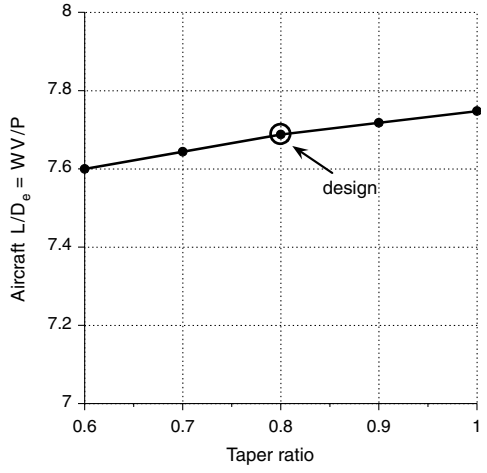

Fig. 16 Effect of blade taper on performance.

the taper was reduced. Although the taper of 1.0 produced the best aircraft lift-to-drag ratio, the taper of 0.8 (tip/root chord) was selected to reduce the blade weight.

Collective pitch of the rotor was varied by 1 deg from −3 to +3 deg to further investigate the effect of the collective pitch (rotor thrust) on the aircraft lift-to-drag ratio, as shown in Fig. 17. The aircraft performance was not sensitive to the collective angle change. The highest aircraft lift-to-drag ratio, which occurred with the −2 deg collective angle, was 0.34% higher than that with the baseline collective angle (0 deg). The aircraft lift-to-drag ratio changed less than 2% with the collective angles investigated.

Aeroelastic Stability

Aeroelastic stability is a very important aspect of the design of helicopters. Stability of a compound helicopter was investigated using the baseline design with disk loading of 15, design blade loading of 0.14, wing loading of 100, collective angle of 0 deg, and $\alpha_w - \alpha_s$ of 3 deg.

Figure 18 shows rotor stability calculations in level flight. Rotor tip speed was varied linearly from the hover value to the cruise value. The corresponding blade frequencies are shown in Fig. 4. The lines in the figure show damping scaled by magnitude. Stability is, in general, insensitive to the speed. No stability issues were observed between 150 and 300 kt.

Figure 19 shows rotor stability at 250 kt with respect to blade frequency change, with the objective of examining the stability characteristics of a compound helicopter with more conventional blade frequency placements. Figure 19a shows rotor stability with respect to the first flap frequency change. In this calculation, a flap hinge and spring stiffness were introduced to change the flap frequency to that of a conventional articulated rotor. Both the lag and torsion stiffness values were maintained the same as the baseline values. The hingeless rotor blade was simulated with a very stiff spring, and the spring stiffness was decreased to reduce the flap frequency. The baseline blade, which was scaled from the LCTC blade design, shows stable modes with the flap frequency change. Figures 19b and 19c show rotor stability with respect to the first lag

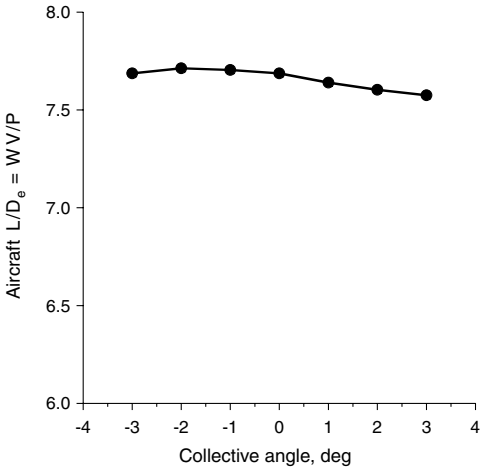

Fig. 17 Effect of collective angle on performance.

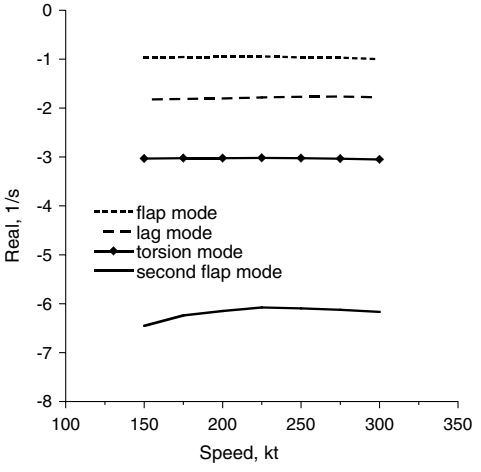

Fig. 18 Cruise stability.

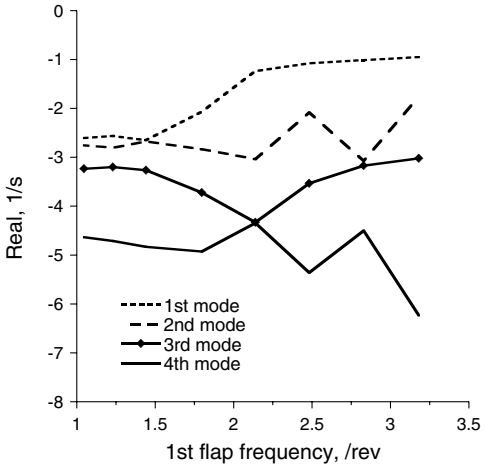

a) First flap frequency change

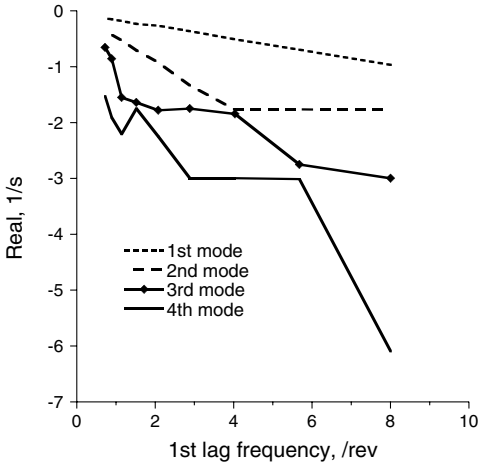

b) First lag frequency change

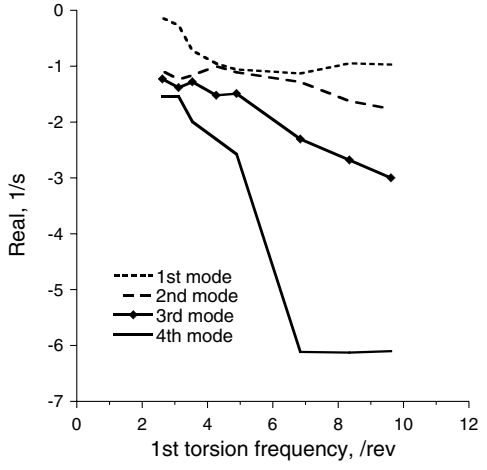

c) First torsion frequency change

Fig. 19 Stability with blade frequency change for baseline aircraft at 250 kt.

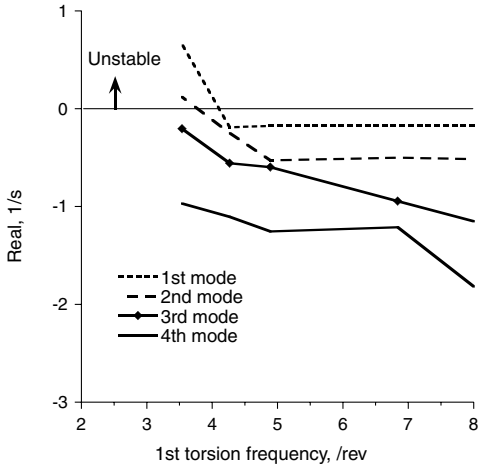

a) Stiff in-plain rotor (ν_ζ = 1.14/rev)

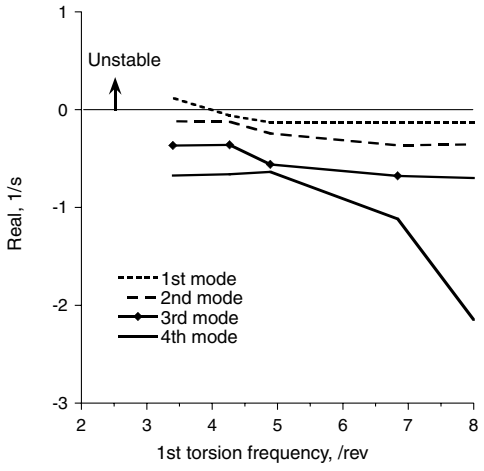

b) Soft in-plain rotor (ν_ζ = 0.71/rev)

Fig. 20 Stability with torsion frequency change for nominal articulated rotor ($\nu_\beta = 1.05/\text{rev}$) at 250 kt.

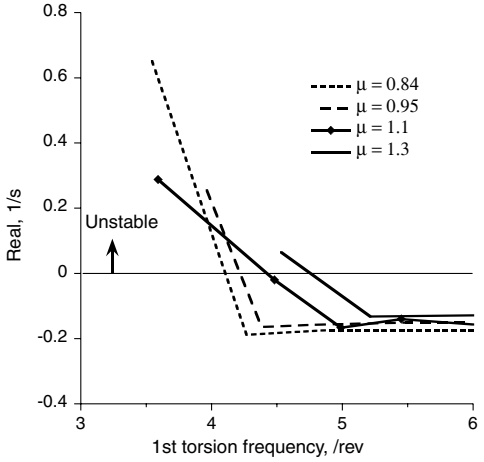

a) Stiff in-plain rotor (ν_ζ = 1.14/rev)

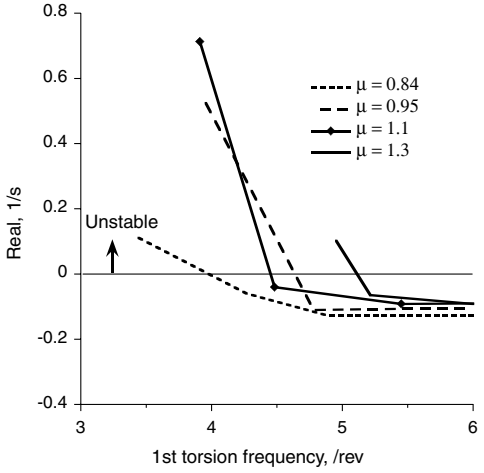

b) Soft in-plain rotor (ν_ζ = 0.71/rev)

Fig. 21 Stability boundary with torsion frequency change for nominal articulated rotor ($\nu_\beta = 1.05/\text{rev}$) at 250 kt with different rotor rpm.

and first torsion frequency change, respectively. Blade lag and torsion stiffness were reduced to obtain lower frequencies, while maintaining the baseline flap frequency. These frequency changes significantly reduced the stability margin, although all the modes were stable within the frequency ranges investigated.

Figure 20 shows rotor stability with respect to the first torsion frequency change at 250 kt for a nominal articulated rotor that has the first flap frequency of 1.05/rev at cruise rpm. Two lag frequencies were investigated: stiff in-plain rotor (1.14/rev) and soft in-plain rotor (0.71/rev). Instability occurred at the first torsion frequency of 4.1/rev for the stiff in-plain rotor and 3.85/rev for the soft in-plain rotor.

Figure 21 shows rotor stability (least damped mode) with respect to the first torsion frequency change at 250 kt for a nominal articulated rotor with the rotor rpm change (thus, an advance ratio change). Again, the two lag frequencies were investigated: stiff in-plain rotor (1.14/rev) and soft in-plain rotor (0.71/rev). In this calculation, both the flap and lag stiffness values were adjusted at different rotor rpm to maintain the same frequencies per revolution. Instability occurred, in general, at a higher first torsion frequency as the advance ratio increased (rotor rpm decreased). The stability boundary is summarized in Table 4.

Rotor Control

Helicopter control requires the ability to produce forces and moments on the vehicle. The changes of hub forces and moments with respect to pilot controls are shown in Fig. 22 as a function of flight speed for the baseline design (high flap frequency). The calculation was carried out for fixed controls, with ±1 deg of collective and cyclic angle change relative to the trimmed solution. The phase shift needed for hingeless rotor control was not considered; longitudinal and lateral cyclic are sine and cosine harmonics of root pitch. Figures 22a and 22b show the hub force and moment change with respect to the collective angle change. As expected, the collective angle changed the vertical force by about 8000–12,000 lb at 175 and 300 kt, respectively. Lateral and longitudinal force change was small. A large roll moment change was observed. This is because the lift increase with the increased collective angle is concentrated on the advancing side due to a large reverse flow region on the retreating side.

Table 4 Stability boundary for nominal articulated rotor ($\nu_\beta = 1.05/\text{rev}$) at 250 kt with different rotor rpm

advance ratio	Rotor rpm	Stability boundary (/rev)
Stiff in-plain rotor ($\nu_\zeta = 1.14/\text{rev}$)		
0.84	104.0	3.85
0.95	92.0	4.64
1.10	80.1	4.45
1.30	68.1	5.11
Soft in-plain rotor ($\nu_\zeta = 0.71/\text{rev}$)		
0.84	104.0	4.11
0.95	92.0	4.37
1.10	80.1	4.42
1.30	68.1	4.76

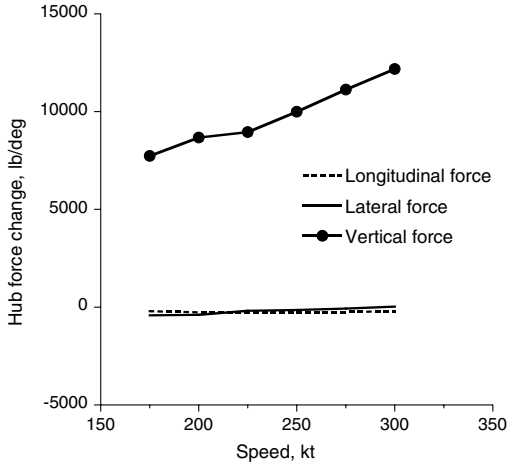

a) Hub force change w.r.t. collective

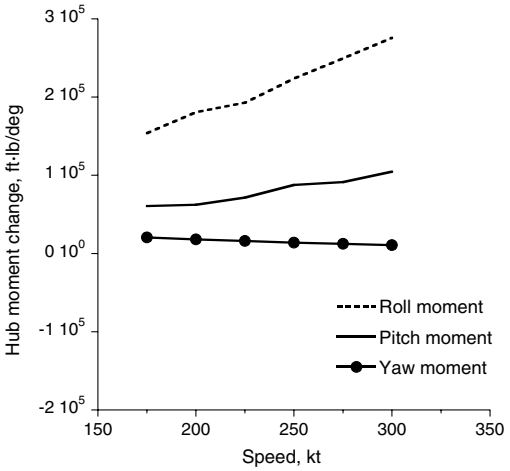

b) Hub moment change w.r.t. collective

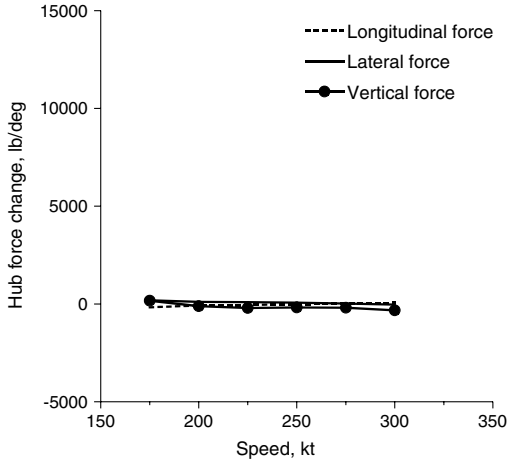

c) Hub force change w.r.t. lateral cyclic

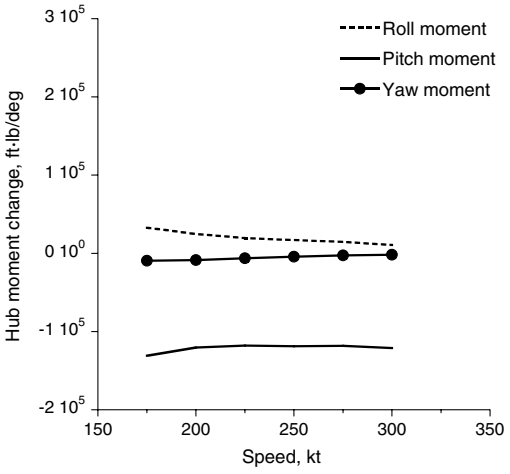

d) Hub moment change w.r.t. lateral cyclic

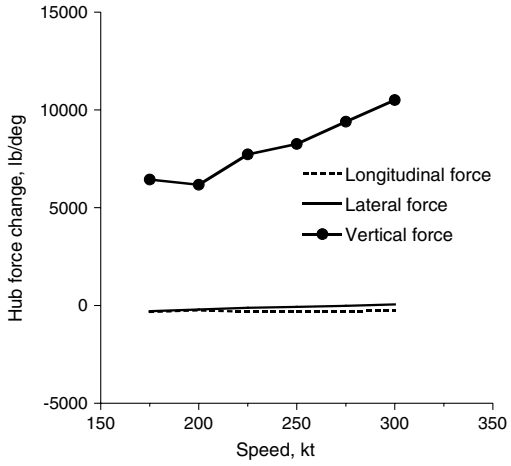

e) Hub force change w.r.t. longitudinal cyclic

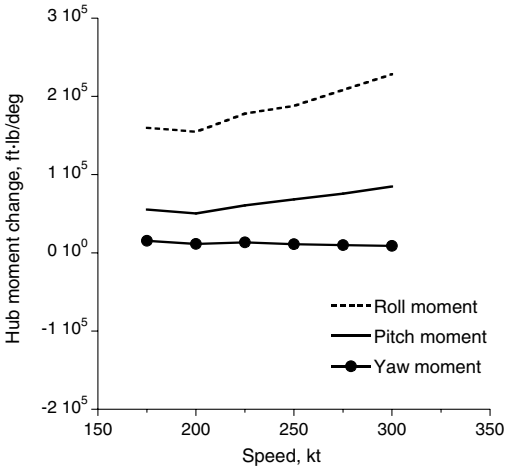

f) Hub moment change w.r.t. longitudinal cyclic

Fig. 22 Hub load change with respect to controls.

Figures 22c and 22d show the hub force and moment change with respect to the lateral cyclic angle change. Hub force change was small. There is a large pitch moment change, as expected.

Figures 22e and 22f show the hub force and moment change with respect to the longitudinal cyclic angle change. The results are quite similar to the hub force and moment change with respect to the collective angle. There are smaller changes in vertical force and roll moment with the longitudinal cyclic change than the collective change.

In summary, for this hingeless rotor, the control derivatives did not change much with speed, but did exhibit significant coupling.

Conclusions

A design and aeromechanics investigation was conducted for a 100,000 lb compound helicopter with a single main rotor that will cruise at a condition of 250 kt at 4000 ft/95°F. Performance,

stability, and control analyses were conducted with the comprehensive rotorcraft analysis CAMRAD II.

Wind-tunnel test measurements of the performance of the H-34 and UH-1D rotors at high advance ratios were compared with calculations to assess the accuracy of the analysis for the design of a high-speed helicopter. In general, good correlation was obtained.

An assessment of the effect of various design parameters (disk loading, design blade loading, wing loading) on the performance of the compound helicopter were made.

1) Lower wing loading (larger wing area) and higher design blade loading (smaller blade chord) increased the aircraft lift-to-drag ratio. However, disk loading had a small influence on the aircraft lift-to-drag ratio.

2) For the baseline design ($W/A = 15$, $C_W/\sigma = 0.14$, $W/S=$ 100), the optimum lift sharing between the rotor and wing was as follows: the rotor carries 8–9% of the gross weight and the wing carries 91–92% of the gross weight.

3) The optimum aircraft lift-to-drag ratio for the baseline design occurred with a small, positive shaft power to the rotors of between 600 and 800 hp.

A rotor parametric study was conducted to investigate the effects of twist, collective, tip speed, and taper on the aircraft lift-to-drag ratio.

1) Blade twist is a more important parameter with regard to aircraft performance for the current compound helicopter design than the compound helicopter developed in the NASA Heavy Lift Investigation.

2) Most of the benefit of slowing the rotor occurs at the initial 20–30% reduction of the advancing blade-tip Mach number.

3) Aircraft performance is not sensitive to collective angle change.

No stability issues were observed with the current design as long as the torsion frequency was kept above about 4/rev. The control derivatives did not change much with speed, but did exhibit significant coupling.

References

[1] Johnson, W., Yamauchi, G. K., and Watts, M. E., "Design and Technology Requirements for Civil Heavy Lift Rotorcraft," *Proceedings of the American Helicopter Society Vertical Lift Aircraft Design Conference*, American Helicopter Society, Alexandria, VA, Jan. 2006.

[2] Yeo, H., and Johnson, W., "Aeromechanics Analysis of a Heavy Lift Slowed-Rotor Compound Helicopter," *Journal of Aircraft*, Vol. 44, No. 2, March–April 2007, pp. 501–508. doi:10.2514/1.23905

[3] Johnson, W., "Technology Drivers in the Development of CAMRAD II," American Helicopter Society Paper PS.3, Jan. 1994.

[4] Yeo, H., Bousman, W. G., and Johnson, W., "Performance Analysis of a Utility Helicopter with Standard and Advanced Rotor," *Journal of the American Helicopter Society*, Vol. 49, No. 3, July 2004, pp. 250–270. doi:10.4050/JAHS.49.250

[5] Yeo, H., and Johnson, W., "Assessment of Comprehensive Analysis Calculation of Airloads on Helicopter Rotors," *Journal of Aircraft*, Vol. 42, No. 5, Sept.–Oct. 2005, pp. 1218–1228. doi:10.2514/1.11595

[6] Yeo, H., and Johnson, W., "Prediction of Rotor Structural Loads with Comprehensive Analysis," *Journal of the American Helicopter Society*, Vol. 53, No. 2, April 2008, pp. 193–209. doi:10.4050/JAHS.53.193

[7] McCloud, J. L., Biggers, J. C., and Stroub, R. H., "An Investigation of Full-Scale Helicopter Rotors at High Advance Ratios and Advancing Tip Mach Numbers," NASA TN D-4632, July 1968.

[8] Charles, B. D., and Tanner, W. H., "Wind Tunnel Investigation of Semirigid Full-Scale Rotors Operating at High Advance Ratios," United States Army Aviation Materiel Laboratories TR 69-2, Jan. 1969.

[9] Yeo, H., and Johnson, W., "Optimum Design of a Compound Helicopter," American Helicopter Society Paper T111-3, Nov. 2006.

[10] Yeo, H., "Calculation of Rotor Performance and Loads under Stalled Conditions," *Proceedings of the American Helicopter Society 59th Annual Forum*, American Helicopter Society, Alexandria, VA, May 2003, pp. 511–525.